Journal of Applied Mechanics and Technical Physics, Vol. 38, No. 1, 1997

CALCULATION OF FLOWS OF A MEDIUM INDUCED BY HIGH-POWER BEAMS OF CHARGED PARTICLES

A. P. Yalovets

UDC 539.893:539.121.7

Irradiation of solid-state targets by a high-power beam of accelerated charged particles (electrons or ions) with energy-flux density $\geqslant 10^7$ W/cm^2 is accompanied by generation of compression and expansion waves in the radiation-free part of the material due to intense warming up of some volume of the target caused by stoppage of particles. Wave propagation over a solid body causes deformations leading to the formation of various defects [1–4], to changes in the mechanical properties of the material, and even to failure [5].

The system of equations describing the generation and propagation of elastoplastic waves in a material, which are induced by a charged-particle beam, includes a kinetic equation for high-velocity charged particles, equations of continuum mechanics, and a wide-range equation of state.

Experience on the numerical solution of this problem has shown that many calculations deal with the equations of continuum mechanics. To simulate the effect of high-power beams of charged particles on a material, these equations are solved by various methods: Leshkevich and Khalikov et al. in [6, 7] used the method of macroparticles [8], Akkerman et al. in [9, 10] used the Godunov method [11], and Val'chuk in [12] used the Wilkins method [13].

Application of the method of macroparticles to the problem considered here involves two difficulties. First, this method is unstable for weak flows. This does not make it possible to simulate the effect of the beams that are of technological interest and, second, in the free-surface problems the free surfaces are difficult to approximate.

The main drawback of the Godunov method is a strong smoothing of the solution in the vicinity of a contact discontinuity.

The method for solving the equations of continuum mechanics which was developed by Wilkins [13] avoids the drawbacks listed above, although there are some difficulties in its application due to the use of Lagrangian variables to simulate strong deformations of the material.

One more problem, which is common for all schemes containing artificial viscosity, is to select a value of the coefficient of artificial viscosity. Numerical experiments show that with an acceptable smoothness of the solution, variation in this coefficient changes the shock-wave amplitude by 10–20%. In addition, in calculation of flow of a medium that is in the liquid–gas equilibrium region, the schemes with artificial viscosity become unstable because of a large decrease in the sound velocity (by 2–3 orders of magnitude).

In the present paper, we find analytical solutions of the equations of continuum mechanics for a material component by means of which the motion of the entire system is simulated. In some cases, the use of the analytical solutions obtained makes it possible to increase the time step of calculation. This increase can be considerable in comparison to the time step found from the Courant condition, as in the example below.

The equations are solved in Lagrangian variables. The algorithm proposed for reconstruction of the Lagrangian grid, which is based on conservation laws, allows one to calculate strong deformations of the material.

1. Calculation of One-Dimensional Elastoplastic Flows. Let a beam of accelerated charged particles be incident on a flat target with thickness a. The z axis is directed perpendicular to the flat surface of the target. The system of equations we use to simulate one-dimensional nonstationary elastoplastic flows

Chelyabinsk State University, Chelyabinsk 454136. Translated from Prikladnaya Mekhanika i Tekhnicheskaya Fizika, Vol. 38, No. 1, pp. 151–166, January–February, 1997. Original article submitted July 23, 1993; revision submitted January 5, 1996.

0021-8944/97/3801-0137 $18.00

is formulated in [13]. To describe the medium's flows induced by a beam of charged particles, the following function for the rate of specific energy release (energy-release function) should be added to the right-hand side of the equation for internal energy:

$$D(z) = \int\limits_{4\pi} d\Omega \int dT_b B(T_b)\Psi(z, \cos\vartheta, T_b), \tag{1.1}$$

where Ψ is the energy-flux density of high-velocity particles, which is differential with respect to the angle and energy variables, ϑ is the angle between the momentum vector of high-velocity particles and the Oz axis, and $B(T_b)$ are the specific energy losses (per unit mass length) of a particle with kinetic energy T_b. To find the differential flux density, it is necessary to solve the kinetic equation for fast particles [14]:

$$\hat{L}\Psi = S_\Psi. \tag{1.2}$$

Here S_Ψ is a source function of fast particles and $\hat{L}$ is the operator of transfer, which takes into account the processes of elastic and inelastic collisions [14]. The following designations are used below: ρ, v, and U are the mass density of the material, the mass velocity, and the internal energy per unit mass, $\Sigma = -P + s^z$, P is the hydrostatic pressure; s^x, s^y, and s^z are the components of the stress deviator, $2\mu = E/(1+\sigma)$ is the Lamé constant, E is the Young's modulus, and σ is the Poisson's ratio.

We used the wide-range equations of state of [15, 16]. The plastic flow is described by keeping the stress deviator at the yield point (the von Mises yield condition) [13].

As in [13], the domain occupied by the material is divided into cells, with the mass, density, stress, and energy determined at the centers of the cells and with the velocity determined at their boundaries. For a concrete cell, the system formulated above can be written in the form

$$\dot{v}_i = (\Sigma_{i+1/2} - \Sigma_{i-1/2})/m_i, \quad m_i = 0.5(m_{i+1/2} + m_{i-1/2}); \tag{1.3}$$

$$\dot{\xi}_{i+1/2} = v_{i+1} - v_{i-1}, \quad \xi_{i+1/2} = m_{i+1/2}/\rho_{i+1/2}; \tag{1.4}$$

$$\dot{U}_{i+1/2} = \Sigma_{i+1/2}\dot{\xi}_{i+1/2}/m_{i+1/2} + D_{i+1/2}; \tag{1.5}$$

$$\dot{s}^z_{i+1/2} = (4\mu/3)\dot{\xi}_{i+1/2}/\xi_{i+1/2}, \quad \dot{s}^x_{i+1/2} = \dot{s}^y_{i+1/2} = -(2\mu/3)\dot{\xi}_{i+1/2}/\xi_{i+1/2}, \tag{1.6}$$

where $m_{i+1/2}$ is the mass of the material in the cell, $\xi_{i+1/2} = z_{i+1} - z_{i-1}$ is the width (volume) of the cell, and $D_{i+1/2}$ is calculated using (1.1) for $z_{i+1/2} = 0.5(z_{i+1} + z_{i-1})$.

We shall find an approximate analytical solution of Eqs. (1.3)–(1.6) at the time step $t_{n+1} - t_n$, assuming that during this time the material in the cell varies adiabatically. Variation in the internal energy due to the particle stoppage in the cell can be taken into account at the end of the time interval considered.

We represent the stress as a function of the volume by the following Taylor series up to the first order for small times:

$$\Sigma(\xi_{i+1/2}) = \Sigma^n_{i+1/2} + (c^n_s)^2_{i+1/2}\rho^n_{i+1/2}\frac{\xi_{i+1/2} - \xi^n_{i+1/2}}{\xi^n_{i+1/2}}. \tag{1.7}$$

Here $c_s^2 = c^2 - (\partial s^z/\partial\rho)_S$, $c = (\partial P/\partial\rho)_S^{1/2}$ is the local sound velocity, S is the entropy, $\Sigma^n_{i+1/2} = \Sigma(\xi^n_{i+1/2})$, $\xi^n_{i+1/2} = \xi_{i+1/2}(t_n)$, $\xi_{i+1/2} = \xi_{i+1/2}(t)$, and $t \geqslant t_n$.

Substituting (1.7) into Eq. (1.3) and differentiating the expression obtained once again with respect to time, we have

$$\ddot{v}_i = \frac{1}{m_i}\left[\left(c_s^2\frac{\rho}{\xi}\right)^n_{i+1/2}\dot{\xi}_{i+1/2} - \left(c_s^2\frac{\rho}{\xi}\right)^n_{i-1/2}\dot{\xi}_{i-1/2}\right]. \tag{1.8}$$

From Eq. (1.8) and the continuity equation (1.4) it follows that

$$\ddot{v}_i + \omega_i^2 v_i = L_i, \tag{1.9}$$

where

$$\omega_i^2 = 2\frac{m_{i+1/2}\,\omega_{i+1/2}^2 + m_{i-1/2}\,\omega_{i-1/2}^2}{m_{i+1/2} + m_{i-1/2}}; \quad \omega_{i+1/2}^2 = (c_s^2\rho/m\xi)_{i+1/2}^n;$$

$$L_i = (m_{i+1/2}\,\omega_{i+1/2}^2\,v_{i+1} + m_{i-1/2}\,\omega_{i-1/2}^2\,v_{i-1})/m_i.$$

The initial conditions for (1.9) have the form

$$v_i(t_n) = v_i^n, \quad \dot{v}_i(t_n) = \dot{v}_i^n = (\Sigma_{i+1/2}^n - \Sigma_{i-1/2}^n)/m_i. \tag{1.10}$$

For all i, Eq. (1.9) is a closed system, whose solution would allow one to find the velocities at all cell boundaries. However, for a large number of cells, this solution is of a rather complicated form.

Assuming that the right-hand side of Eq. (1.9) remains constant for the integration step and is equal to L_i^n, and using the initial conditions (1.10), we can obtain the following analytical solution:

$$v_i(t) = v_i^n \cos(\omega_i\tau) + \dot{v}_i^n \frac{\sin(\omega_i\tau)}{\omega_i} + L_i^n \frac{1-\cos(\omega_i\tau)}{\omega_i^2}, \tag{1.11}$$

where $\tau = t - t_n$.

Integration of (1.11) over time between t_n and t makes it possible to calculate the coordinates of the cell boundaries:

$$z_i(t) = z_i^n + v_i^n \frac{\sin(\omega_i\tau)}{\omega_i} + \dot{v}_i^n \frac{1-\cos(\omega_i\tau)}{\omega_i^2} + \frac{L_i^n}{\omega_i^2}\left(\tau - \frac{\sin(\omega_i\tau)}{\omega_i}\right). \tag{1.12}$$

Taking into account expansion (1.7) and solution (1.12), it is not difficult to integrate Eq. (1.5):

$$U_{i+1/2}(t) = \left[U^n + \frac{\Sigma^n}{m}(\xi - \xi^n) + \frac{\omega^2}{2}(\xi - \xi^n)^2 + D\tau\right]_{i+1/2}. \tag{1.13}$$

The expressions for new values of the deviator are found by solution of (1.6):

$$\begin{aligned} s_{i+1/2}^z(t) &= s_{i+1/2}^z(t_n) + (4\mu/3)(\xi_{i+1/2}/\xi_{i+1/2}^n - 1), \\ s_{i+1/2}^x(t) &= s_{i+1/2}^y(t) = s_{i+1/2}^x(t_n) - (2\mu/3)(\xi_{i+1/2}/\xi_{i+1/2}^n - 1). \end{aligned} \tag{1.14}$$

The von Mises yield condition is satisfied, as in [13].

A new value of the medium's density is found from the expression

$$\rho_{i+1/2}(t) = m_{i+1/2}/\xi_{i+1/2}, \tag{1.15}$$

and a new value of the hydrostatic pressure is found from the equation of state using the internal energy and the mass density (1.15) obtained from (1.13). Ignoring the density dependence of μ, from (1.14) we have $c_s^2 = c^2 + 4\mu/3\rho^n$.

If the stresses exceed the yield point in absolute value, $c_s^2 = 0$ under expansion and $c_s^2 = c^2$ under compression.

The time step τ is determined by approximations that were made in the derivation of formulas (1.11)–(1.15). The first approximation consists in the use of expansion (1.7), from which follows

$$|\Delta\xi/\xi| \leqslant \varepsilon, \tag{1.16}$$

where ε is the maximum admissible relative variation in the cell volume on the time step, which ensures the validity of expansion (1.7). From relation (1.16) and the continuity equation (1.4) it follows that

$$\tau \leqslant (\varepsilon\xi/|\Delta v|)_{\min}, \quad \Delta v = v_{i+1} - v_i. \tag{1.17}$$

The second approximation consists in the replacement of the right-hand side of (1.9) by a constant. We have, however, failed to obtain a simple criterion for the time step in this case. Numerical experiments have shown that the choice of the time step via (1.17) usually yields good results. For small velocity gradients,

the value of τ increases to such an extent that the error attributed to the approximate solution of Eq. (1.9) becomes significant. Therefore, in practice one more condition is imposed on the time step for $\tau > \tau_C$:

$$\tau/\tau_C \leqslant N, \tag{1.18}$$

where τ_C is the time step found from the Courant condition [13], and N is a quantity larger than unity.

One important remark concerning the use of formulas (1.11)–(1.13) should be made. Equation (1.9) describes the motion of two oscillators with natural frequencies $\omega_{i-1/2}$ and $\omega_{i+1/2}$. The expression for $\omega_{i+1/2}$ contains $\xi_{i+1/2}$, which is the cell width [formula (1.9)]. Under compression of the cell, not the entire layer of material contained in the cell volume is perturbed, but only the layer $c\tau$. The natural frequency of the cell should, therefore, be calculated by the formula

$$\omega^2_{i+1/2} = (c_s^2\rho/m\tilde{\xi})^n_{i+1/2}, \tag{1.19}$$

where

$$\tilde{\xi}^n_{i+1/2} = \begin{cases} \xi_{i+1/2}, & \dot{\xi}_{i+1/2} \geqslant 0, \\ c_{i+1/2}\tau, & \dot{\xi}_{i+1/2} < 0. \end{cases}$$

We shall consider the case of small τ. Let us expand (1.11) into a Taylor series in terms of time up to the second order and ignore the stress deviator for simplicity. Substituting the explicit form of L^n_i into the expression obtained, we have

$$v_i^{n+1} = v_i^n - [(P^n_{i+1/2} + q^n_{i+1/2}) - (P^n_{i-1/2} + q^n_{i-1/2})]\tau/m_i, \tag{1.20}$$

where $q^n_{i+1/2} = -m_{i+1/2}\,\omega^2_{i+1/2}\,(v^n_{i+1} - v^n_i)\,\tau/2$. Under compression of the cell, when $v^n_{i+1} - v^n_i < 0$, with allowance for (1.19), the quantity $q^n_{i+1/2} = c_{i+1/2}\,\rho^n_{i+1/2}|v^n_{i+1} - v^n_i|/2$ has the form of linear artificial viscosity [8, 13].

This analysis has shown that the artificial viscosity introduced into various numerical schemes allows virtually an approximate allowance, on the time step, for the dependence of the pressure in the element of material on the volume and also takes into account the irreversibility of real physical processes, which were initially described by reversible differential equations. Here the irreversibility of the physical processes is taken into account by expression (1.19).

Under expansion of the material, the artificial viscosity is assumed to be equal to zero, although, as follows from (1.19) and (1.20), $q^n_{i+1/2} = -(c^2\rho^n\Delta\xi/2\,\xi)_{i+1/2}$.

Let us investigate the dispersive and dissipative properties of the solution obtained. For this purpose, we consider the propagation of the Fourier mode of the mass velocity $v(z,t) = \hat{v}\exp(i\omega t - kz)$ in a homogeneous medium, when $\Sigma_{i+1/2} - \Sigma_{i-1/2} = 0$. In this case, the dispersion relation

$$\exp(i\omega\tau) = \cos(\omega_i\tau) + (1 - \cos(\omega_i\tau))\cos(k\xi) \tag{1.21}$$

can be obtained from (1.11).

Since the imaginary part in (1.21) is equal to zero, wave dispersion is absent. The dissipative properties of the scheme are determined by the modulus of expression (1.21). A necessary and sufficient condition for stability of the solution is $|\cos(\omega_i\tau) + (1 - \cos(\omega_i\tau))\cos(k\xi)| \leqslant 1$. This condition is satisfied for all k if $\omega_i\tau \leqslant \pi/2$. This is possible for values of τ exceeding τ_C by a factor of 1.5, i.e., $N \leqslant 1.5$. When long-wave harmonics prevail in the solution, as, for example, in the problem of gas motion in a vacuum, the stability condition can be satisfied at larger values of N as well. The absence of attenuation of waves whose wave length can be placed an integer number of times on the grid size allows accurate computation of discontinuities.

The multistep method of [17] is used to solve the kinetic equation (1.2). A detailed description of this method is given for one-dimensional geometry in [12], and for two-dimensional geometry in [18]. The model of electron transfer takes into account fluctuations of energy losses in inelastic collisions, radiation deceleration, and elastic scattering, in accordance with the Gaudsmith–Saunderson multiple scattering theory (realized using the formulas of [19]). The model of ion transfer incorporates fluctuations in inelastic collisions, but ignores elastic scattering and nuclear reactions. The energy losses of ions are calculated on the basis of the data of [20].

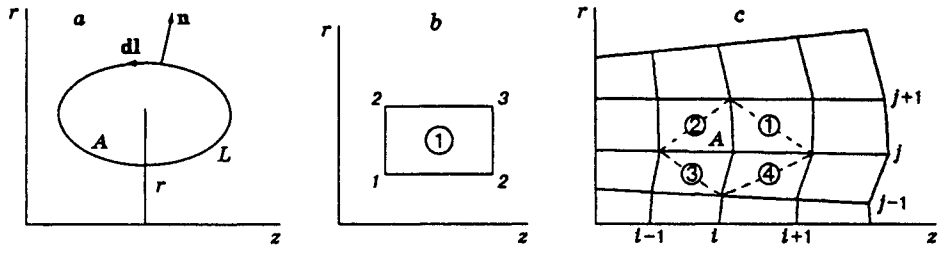

Fig. 1

2. Calculation of Two-Dimensional Hydrodynamic Flows. In the case of the action of a focused beam of accelerated charged particles on a target whose dimensions are greater than the beam radius, solution of the problem in one-dimensional geometry becomes unacceptable and requires at least the two-dimensional geometry.

Only the hydrostatic pressure is taken into account in the present paper to simplify the presentation of the method. This is valid for beams with energy-flux density $\geqslant 10^{10}$ W/cm^2, when the values of the resulting pressure in the material exceed considerably the yield point. The system of equations governing the fluid motion in the hydrodynamic approximation for cylindrical geometry contains
the equations of motion

$$\dot{v}^r = -\rho^{-1}\partial P/\partial r, \quad \dot{v}^z = -\rho^{-1}\partial P/\partial z, \tag{2.1}$$

the continuity equation

$$\dot{V}/V = (\nabla \mathbf{v}), \tag{2.2}$$

the equation for internal energy

$$\dot{U} = -P\dot{V}/(\rho V) + D, \tag{2.3}$$

the equation of state, and the kinetic equation to calculate the function of energy release. Here r and z are the coordinates, v^r and v^z are the components of the mass velocity of the material, and $V = m/\rho$ is the volume of the element of the medium of mass m.

We shall use the integral definition of partial derivatives, as in [13], and write the equations of motion (2.1) for the element of the medium with area A in the form (Fig. 1a)

$$\dot{v}^r = r \oint_L P dl_z/M, \quad \dot{v}^z = -r \oint_L P dl_r/M, \tag{2.4}$$

where L is the boundary of the element A, $M = rA\rho$ is the mass of the material in A, and dl_r and dl_z are the projections of a contour element $\mathbf{dl}$ onto the axis of the cylindrical system of coordinates.

Let us write the continuity equation for the element A using the Ostrogradskii–Gauss divergence theorem in the form

$$\dot{V} = \oint_L (\mathbf{vn}) r dl \tag{2.5}$$

($\mathbf{n}$ is the normal to $\mathbf{dl}$).

The equation for the internal energy of the element A is represented as

$$\dot{U} = -P\dot{V}/M + D. \tag{2.6}$$

We seek an approximate analytical solution of Eqs. (2.1)–(2.6) at the time step $t_{n+1} - t_n$. In the adiabatic case, the pressure versus the volume can be represented in the vicinity of some V^n as the Taylor expansion:

$$P(V) = P^n - Q^n(V - V^n), \tag{2.7}$$

where $Q = c^2\rho/V$ and $P^n = P(V^n)$. Substituting (2.7) into (2.4) and differentiating the expression obtained with respect to time once again, for the velocity components we have

$$\ddot{v}^r = v^r \oint_L P^n dl_z/M - r \oint_L Q^n \dot{V} dl_z/M, \quad \ddot{v}^z = -v^r \oint_L P^n dl_r/M + r \oint_L Q^n \dot{V} dl_r/M. \tag{2.8}$$

In Eqs. (2.8), the terms $v^r \oint_L Q^n(V - V^n) dl_{r,z}$ are ignored, because their ratio to $r \oint_L Q^n \dot{V} dl_{r,z}$ is considerably smaller than unity.

Substitution of the continuity equation (2.5) into (2.8) makes it possible to find equations for the velocity components of the element of the medium, in which the thermodynamic properties of the material are given at the surface of this element.

To obtain a system of equations governing the motion of the entire medium, a grid is marked on the domain occupied by the medium and this domain is divided into quadrilaterals (Fig. 1b). In what follows, the notation of [13] is used. The centers of the quadrilaterals have, in fractions of the cell sizes, the following coordinates:

$$①\equiv j+1/2,\ i+1/2,\quad ②\equiv j+1/2,\ i-1/2,\quad ③\equiv j-1/2,\ i-1/2,\quad ④\equiv j-1/2,\ i+1/2.$$

The thermodynamic characteristics of the material are determined at the centers of the cells. Thus, we denote the density, mass, volume, pressure, and internal energy at the point ① by $\rho_①$, $M_①$, $V_①$, $P_①$, and $U_①$, respectively. The area, volume, and mass of a cell are determined by the formulas presented in [13].

The continuity equation (2.5) for a single cell can be written in the form (Fig. 1b)

$$\begin{aligned}\dot{V}_① = 0.5\,[&r_1(r_2 - r_4)v_1^z + r_2(r_3 - r_1)v_2^z + r_3(r_4 - r_2)v_1^z + r_4(r_1 - r_3)v_1^z \\ &- r_1(z_2 - z_4)v_1^r - r_2(z_3 - z_1)v_2^r - r_3(z_4 - z_2)v_1^r - r_4(z_1 - z_3)v_1^r],\end{aligned} \tag{2.9}$$

where the subscripts denote the numbers of the cell's vertices (the numbering is counterclockwise).

Calculating the integrals over the contour, which is shown in Fig. 1c by a dashed curve, according to the scheme presented in [13], from (2.8) and (2.9) we obtain

$$\ddot{v}^r_{ji} + \omega_r^2 v^r_{ji} = L_r, \qquad \ddot{v}^z_{ji} + \omega_z^2 v^z_{ji} = L_z. \tag{2.10}$$

Here

$$\omega_r^2 = \tilde{r}_{ji}^2[Q^n_①(z_2 - z_1)^2 + Q^n_②(z_3 - z_2)^2 + Q^n_③(z_4 - z_3)^2 + Q^n_④(z_1 - z_4)^2]/2M_A - f_r;$$

$$f_r = [P^n_①(z_2 - z_1) + P^n_②(z_3 - z_2) + P^n_③(z_4 - z_3) + P^n_④(z_1 - z_4)]/M_A;$$

$$\begin{aligned}L_r = -(\tilde{r}_{ji}/M_A)\{&Q^n_①(z_2 - z_1)[\dot{V}_① - r_{ji}v^r_{ji}(z_2 - z_1)/2] + Q^n_②(z_3 - z_2)[\dot{V}_② - r_{ji}v^r_{ji}(z_3 - z_2)/2] \\ &+ Q^n_③(z_4 - z_3)[\dot{V}_③ - r_{ji}v^r_{ji}(z_4 - z_3)/2] + Q^n_④(z_1 - z_4)[\dot{V}_④ - r_{ji}v^r_{ji}(z_1 - z_4)/2]\};\end{aligned}$$

$$\omega_z^2 = \tilde{r}_{ji}^2[Q^n_①(r_2 - r_1)^2 + Q^n_②(r_3 - r_2)^2 + Q^n_③(r_4 - r_3)^2 + Q^n_④(r_1 - r_4)^2]/2M_A;$$

$$f_z = [P^n_①(r_2 - r_1) + P^n_②(r_3 - r_2) + P^n_③(r_4 - r_3) + P^n_④(r_1 - r_4)]/M_A;$$

$$\begin{aligned}L_z = (\tilde{r}_{ji}/M_A)\{&Q^n_①(r_2 - r_1)[\dot{V}_① - r_{ji}v^z_{ji}(r_2 - r_1)/2] + Q^n_②(r_3 - r_2)[\dot{V}_② - r_{ji}v^z_{ji}(r_3 - r_2)/2] \\ &+ Q^n_③(r_4 - r_3)[\dot{V}_③ - r_{ji}v^z_{ji}(r_4 - r_3)/2] + Q^n_④(r_1 - r_4)[\dot{V}_④ - r_{ji}v^z_{ji}(r_1 - r_4)/2]\} - v^r_{ji}f_z;\end{aligned}$$

$$M_A = (M_① + M_② + M_③ + M_④)/2; \qquad \tilde{r}_{ji} = V_A/A.$$

The velocity components and their derivatives at time t_n

$$\dot{v}^r_{ji}(t_n) = (\tilde{r}_{ji}f_r)^n, \qquad \dot{v}^z_{ji}(t_n) = -(\tilde{r}_{ji}f_z)^n \tag{2.11}$$

are used as initial conditions for (2.10).

An analytical solution of (2.10) with initial conditions (2.11) can be found similarly to solution of Eq. (1.14). Assuming that the values of ω_r, ω_z, L_r, and L_z remain constant at the time step and are equal to the values at instant t_n, we obtain

$$v_{ji}^r(t) = v_{ji}^r(t_n)C(\omega_r^n\tau) + \dot{v}_{ji}^r(t_n)\frac{S(\omega_r^n\tau)}{\omega_r^n} + L_r^n\frac{1-C(\omega_r^n\tau)}{(\omega_r^n)^2},$$
$$v_{ji}^z(t) = v_{ji}^z(t_n)\cos(\omega_z^n\tau) + \dot{v}_{ji}^z(t_n)\frac{\sin(\omega_z^n\tau)}{\omega_z^n} + L_z^n\frac{1-\cos(\omega_z^n\tau)}{(\omega_z^n)^2}, \tag{2.12}$$

where $\omega = \sqrt{|\omega^2|}$.

$$C(\omega\tau) = \begin{cases} \cos(\omega\tau), & \omega^2 \geqslant 0, \\ \cosh(\omega\tau), & \omega^2 < 0; \end{cases} \qquad S(\omega\tau) = \begin{cases} \sin(\omega\tau), & \omega^2 \geqslant 0, \\ \sinh(\omega\tau), & \omega^2 < 0. \end{cases}$$

Integrating (2.11) with respect to the time from t_n to $t > t_n$, we find the following new coordinates of the nodes:

$$r_{ji}(t) = r_{ji}^n + v_{ji}^r(t_n)\frac{S(\omega_r^n\tau)}{\omega_r^n} + \dot{v}_{ji}^r(t_n)\frac{1-C(\omega_r^n\tau)}{(\omega_r^n)^2} + \frac{L_r^n}{(\omega_r^n)^2}\left(\tau - \frac{S(\omega_r^n\tau)}{\omega_r^n}\right),$$
$$z_{ji}(t) = z_{ji}^n + v_{ji}^z(t_n)\frac{\sin(\omega_z^n\tau)}{\omega_z^n} + \dot{v}_{ji}^z(t_n)\frac{1-\cos(\omega_z^n\tau)}{(\omega_z^n)^2} + \frac{L_z^n}{(\omega_z^n)^2}\left(\tau - \frac{\sin(\omega_z^n\tau)}{\omega_z^n}\right). \tag{2.13}$$

Knowing the new coordinates of the grid nodes, we can calculate a new volume of the cell and, consequently, a new value of density.

Integrating (2.6) together with (2.7), we have

$$U_{①}(t) = [U^n - P^n\Delta V/M + Q^n(\Delta V)^2/2M + D\tau]_{①} \quad [\Delta V_{①} = V_{①}(t) - V_{①}^n]. \tag{2.14}$$

A new value of pressure is found from the equation of state using the obtained values of the internal energy and of the mass density.

As in the one-dimensional case, the time step is found from (1.18), and from the condition $|\dot{V}\tau/V| \leqslant \varepsilon$.

In calculations by formulas (2.12)–(2.14), it is necessary to take into account in the expressions for Q^n that under compression of the element of the material volume only the part of it is perturbed which is determined by the sound velocity and by the compression time. Similarly to (1.24), we write

$$Q^n = (c^2\rho/\tilde{V})^n. \tag{2.15}$$

Here $\tilde{V} = V$ if $\dot{V}^z = \partial v^z/\partial z \geqslant 0$ and $\dot{V}^r = \partial v^r/\partial r + v^r/r \geqslant 0$; otherwise $\tilde{V} = V^{\text{eff}}$.

If the cell is compressed along the z axis, for $\dot{V}^z < 0$, its effective volume can be determined, as in the one-dimensional case, by replacement of the characteristic cell size by $c\tau$:

$$V^{\text{eff}} = Vc\tau A^{-1/2} \tag{2.16}$$

($A^{1/2}$ is the characteristic cell size). The value of $\dot{V}^z$ for the cell can be found using the integral definition of partial derivatives. This leads to an expression equivalent to a part of (2.9) that contains the velocity components v^z.

When the cell volume decreases owing to its deformation and displacement along the r axis ($\dot{V}^r < 0$), $V^{\text{eff}} = Vc^2\tau\tau' A^{-1}$. Here τ' is the effective time of decrease in the cell volume due to its displacement along r: $\tau' = |V/\dot{V}^r|$. The expression for the effective volume in this case has the form

$$V^{\text{eff}} = Vc^2\tau A^{-1}|V/\dot{V}^r|. \tag{2.17}$$

The quantity $\dot{V}^r = \dot{V} - \dot{V}^z$ and, consequently, it is equivalent to the part of (2.9) that contains the velocity components v^r.

Formulas (2.12) and (2.13) make it possible to consider the motion of the grid nodes as a sequential motion of them along the r and z axes. Therefore, expressions (2.15) and (2.17) should be used to calculate ω_r and L_r, and expressions (2.15) and (2.16) should be used to calculate ω_z and L_z. It follows that in (2.14),

the expression $Q(\Delta V)^2$ should be replaced by $Q_z(\Delta V^z)^2 + Q_r(\Delta V^r)^2$, where Q_z and Q_r are calculated by formula (2.15) and, respectively, by formulas (2.16) and (2.17), and

$$\Delta V^z = V(r^{n+1}, z^{n+1}) - V(r^{n+1}, z^n), \qquad \Delta V^r = V(r^{n+1}, z^n) - V(r^n, z^n).$$

Expanding expressions (2.12) into a Taylor series with respect to the time and up to the order $\sim\tau^2$, we obtain

$$v^r(t_{n+1}) \simeq v^r(t_n) + \tau(r^{(n+1/2)}/M_A)\oint(P^n + q^n)dl_z, \quad v^z(t_{n+1}) \simeq v^z(t_n) - \tau(r^{(n+1/2)}/M_A)\oint(P^n + q^n)dl_r$$

($q^n = -Q^n\dot{V}^n\tau/2$). With allowance for (2.15), for $\dot{V}^r < 0$ the quantity q has the form

$$q = (\rho A/2)(\dot{V}/V)^2, \tag{2.18}$$

and for $\dot{V}^z < 0$,

$$q = (c\rho A^{1/2}/2)|\dot{V}/V|. \tag{2.19}$$

Formulas (2.18) and (2.19) correspond, up to constants, to the expressions for artificial (quadratic and linear) viscosity, which is introduced for stability into various numerical schemes [8, 13].

In multidimensional calculations with use of the Lagrangian methods, the grid can be strongly distorted. If the grid is not reconstructed, calculations on the distorted grid can produce a large error, which ultimately leads to instability of the solution. A conventional approach to solution of this problem is to change the structure of the grid nodes, when local distortions of the grid are reduced owing to the introduction of new nodes and the elimination of the previous ones [21]. The construction and realization of such algorithms is, however, a complicated problem.

The method of reconstructing a Lagrangian grid in the problems of collision of bodies is described in [22, 23]. It is oriented, however, to the cases where the region of strong deformations is much smaller than the entire computational domain. In the problems on the effect of charged-particle beams on the material, the region of strong deformations can occupy a considerable part of the entire computational domain, and the method of [22, 23] is difficult to use.

We realize here a method of grid reconstruction that differs from the method of [22, 23] in that a new grid is marked on the entire computational domain. The recalculation of all the parameters of the medium for the new grid is based, as in [22, 23], on the laws of conservation of energy and mass. The law of conservation of momentum is used to calculate the velocities at the nodes of the new grid, whereas in [22, 23] the velocities are calculated by the formulas of linear interpolation. This method reconstructs the regular grid in the entire computational domain without violation of the conservation laws.

Let us calculate the density and internal-energy values at the centers of the new cells $j' + 1/2$ and $i' + 1/2$ and the velocity values at the nodes j' and i' of the new grid. The laws of conservation of mass and total energy allow us to write

$$\rho_{j'+1/2,i'+1/2} = \sum_{\textcircled{k}} \rho_{\textcircled{k}}\Delta\tilde{V}_{\textcircled{k}}/V_{j'+1/2,i'+1/2}, \quad E_{j'+1/2,i'+1/2} = \sum_{\textcircled{k}} \rho_{\textcircled{k}}\Delta\tilde{V}_{\textcircled{k}}E_{\textcircled{k}}/\sum_{\textcircled{k}} \rho_{\textcircled{k}}\Delta\tilde{V}_{\textcircled{k}}, \tag{2.20}$$

where $E_{\textcircled{k}} = U_{\textcircled{k}} + v^2_{\textcircled{k}}/2$; summation is performed over the old cells, which have a common area $\Delta\tilde{V}$ with the new cell $j' + 1/2$ and $i' + 1/2$.

We determine the kinetic energy per unit mass of a cell $v^2_{\textcircled{k}}/2$. From the equation of motion (2.4) written for the material element A (Fig. 1c), it follows that the kinetic energy of this element is equal to $M_A v^2_{ji}/2$. Taking into account the expression for M_A in formulas (2.10), the quantity $M_{\textcircled{1}}v^2_{ji}/4$ can be regarded as a contribution of a separate Lagrangian cell to the kinetic energy of the element A, and the specific kinetic energy of the cell can be found from the expression

$$v^2_{\textcircled{1}}/2 = (v^2_{ji} + v^2_{j,i+1} + v^2_{j+1,i+1} + v^2_{j+1,i})/8. \tag{2.21}$$

To recalculate the velocity field, auxiliary grids for the old and new grids are constructed so that their nodes are the centers of the basic grids. The law of conservation of momentum makes it possible to write for

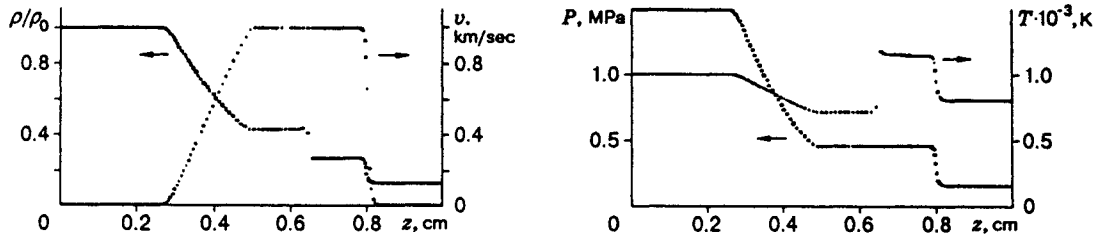

Fig. 2

the auxiliary grids an expression similar to (2.20) in the form

$$v_{j'i'} = \sum_{ji} v_{ji}\rho_{ji}\Delta\tilde{V}_{ji} / \sum_{ji} \rho_{ji}\Delta\tilde{V}_{ji}, \tag{2.22}$$

where summation is performed over the old auxiliary cells which have a common area $\Delta\tilde{V}$ with a new auxiliary cell $j'i'$, and $\rho_{ji} = M_A/V_A$.

The internal energy for new cells $j' + 1/2$ and $i' + 1/2$ is equal to the difference between the total energy obtained by (2.20) and the specific kinetic energy of the new cell calculated by formula (2.21) using the velocities at the nodes $j'i'$.

A practical realization of the grid-reconstruction algorithm described has shown that the use of formulas (2.20)–(2.22) ensures satisfaction of the laws of conservation of mass, momentum, and energy with accuracy 1% or higher even in the solution of problems for which several dozens of procedures of grid reconstruction are required.

3. Numerical Results. The calculations are tested on problems that have self-similar solutions or numerical solutions obtained by another method.

As the first test, the problem of the gas motion in a vacuum was solved with the following parameters: the specific heat ratio was $\gamma = 5/3$, the initial temperature was $T = 1000$ K, the initial density was 1.29 kg/m^3, and the thickness of the layer was 2 cm. With the number of cells equal to 200 and $\varepsilon = 0.02$, after ten time steps the numerical solution approached the self-similar solution. The difference in the gas speed at the front was ~2%. The differences in the mass density, temperature, and sound velocity was not more than 10%. After 100 time steps the difference in the gas speed at the front was 1%, and the distributions of the macroscopic parameters in depth differed by not more than 3%. Investigation of the gas motion during several hundreds of time steps has shown that the energy of the entire gas volume and the entropy of each cell are satisfied with high degree of accuracy (up to three significant digits).

It should be noted that in solving the problem of the gas motion in a vacuum, the choice of the time step from condition (1.17) makes it possible to advance in time, in a certain number of steps, much farther than with the time step chosen from the Courant condition. In this case, in 200 steps the Courant condition made it possible to advance to the moment $t = 0.25$ μsec, while condition (1.17) allowed us to move forward to $t = 1.85$ μsec.

The results of solution of the problem of discontinuity decay for $t = 1.65$ μsec are presented in Fig. 2. The initial state of the gas is as follows: $v_1 = 0$, $\rho_1 = 1$, $T_1 = 1000$ K, $v_2 = 0$, $\rho_2 = 0.125$, $T_2 = 800$ K, and the specific heat ratio $\gamma = 7/5$. This method describes well the contact discontinuity. In solving the problem of discontinuity decay, the law of conservation of energy is conserved with accuracy of 1% or higher. In the quality of description of macroscopic parameters, this calculation corresponds to the SUPERBEE method [24], which was applied to solution of a similar problem (see [21]). It should be noted that this method is constructed such that it solves the Riemann problem accurately.

In this problem, the time step found from (1.17) corresponded to the time step found from the Courant condition.

Figure 3 shows the results of numerical modeling, with the equations of state from [13], of a high-speed impact of an aluminum plate 0.5 cm thick moving at an initial speed of 800 m/sec against an aluminum

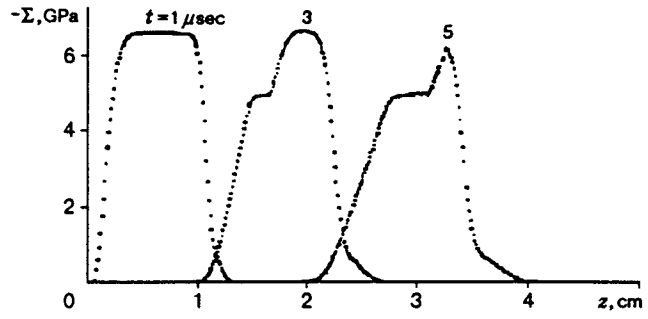

Fig. 3

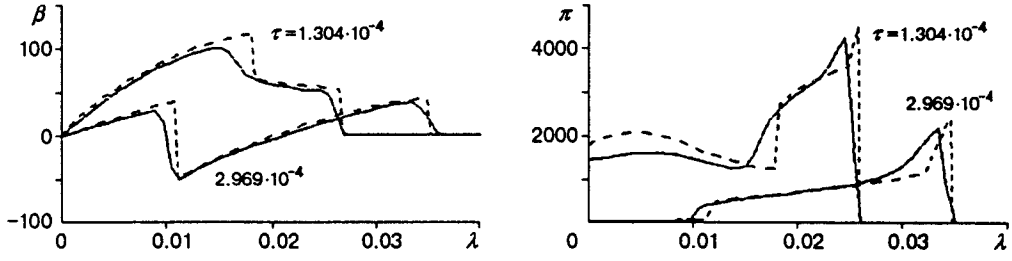

Fig. 4

barrier. Since solid bodies are more rigid than gases, the value of ε from formula (1.17) should be decreased (here $\varepsilon = 0.002$). In high-speed impact calculations, the laws of conservation of energy and momentum were satisfied in the same manner as in solving the previous problems.

It should be noted that in all the cases considered above, an increase in the number of computational nodes by a factor of 2–3 changes the results by not more than 1–2%.

The two-dimensional calculations were tested by solving the one-dimensional problems of the gas motion in a vacuum and of discontinuity decay. The results obtained are in complete agreement with the results of calculations by the one-dimensional program presented here.

We shall demonstrate the effectiveness of the method for solving two-dimensional hydrodynamic equations by an example of solution of the problem of expansion of a high-temperature, high-pressure sphere of air [25]. The initial conditions of this problem included an isothermal sphere of air initially at rest at normal density and with pressure $P_n = 20{,}000$ atm. We used the equation of state for air from [25].

In solving the problem, a 12.5×25 cm domain was considered. The center of the high-pressure sphere of air is at the point $r_0 = 0$, $z_0 = 12.5$ cm, and the initial radius of the sphere was $R_{\text{ini}} = 5$ cm. A uniform 51×101 grid was chosen.

The results of two-dimensional calculations were compared with the results of the one-dimensional calculations of [25], which are represented by distributions $\pi(\lambda) = P/P_0$, $\eta(\lambda) = \rho/\rho_0$, and $\beta(\lambda) = v/c_0$ at various τ. Here $P_0 = 1.01375 \cdot 10^5$ Pa, $\rho_0 = 1.188$ kg/m^3; $c_0 = 346$ m/sec, λ is the distance from the center of explosion in units of $a = (W/P_0)^{1/3}$, W is the energy of explosion, and $\tau = tc_0/a$. In our calculations, the parameter a was found from the relation $a = R_{\text{ini}}/\lambda_0$, where $\lambda_0 = 0.01625$ [25].

Since the Lagrangian cells were strongly distorted in modeling of a spherical shock wave, the grid was reconstructed if at least for one cell the ratio of diagonals was different from unity by an assigned quantity.

The functions $\beta(\lambda)$ and $\pi(\lambda)$ obtained by the two-dimensional program (solid curves) and from the one-dimensional calculations of [25] (dashed curves) for various times τ are compared in Fig. 4.

The isobars presented in Fig. 5 (in gigapascals) at time $\tau = 2.969 \cdot 10^{-4}$ indicate a satisfactory description of the spherical symmetry.

The results of the two-dimensional calculation for the problem of expansion of a high-temperature, high-

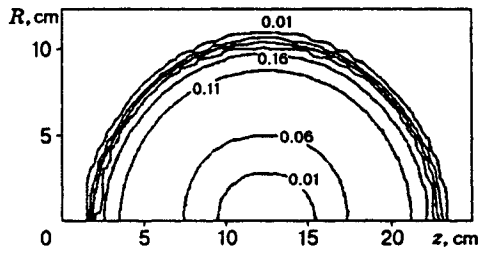

Fig. 5

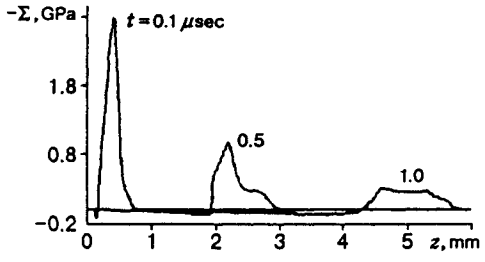

Fig. 6

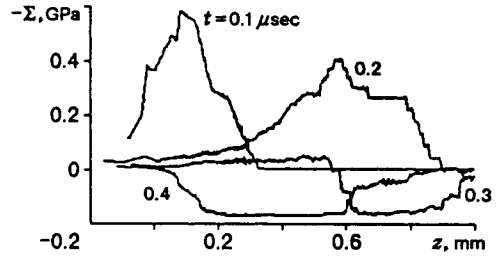

Fig. 7

pressure sphere of air presented here demonstrate the applicability of the method developed for solving the hydrodynamic equations to simulation of spatial distributions of the macroscopic parameters of the medium in the presence of strong deformations.

As a result of beam-particle deceleration, intense heating of the material and formation of a high-pressure region occur. Unloading of the compressed material is accompanied by stress-wave propagation over the target volume. Generation of stress waves in a material under irradiation by electron or ion beams with an energy-flux density of $\sim 10^7$–10^9 W/cm^2 and a pulse duration of $\sim 10^{-7}$–10^{-6} sec is most interesting for technological purposes.

We demonstrate some calculation results of the stress fields in the solid-state part of a target under the action of high-power beams of charged particles. The calculations are carried out using the wide-range equations of state of [16].

Figure 6 shows the stress profiles in an iron target 5 mm thick at various times under irradiation by a pulsed electron beam. The pulse duration is 100 nsec, the duration of the leading and trailing edges of the current and voltage pulses is 10 nsec, the maximum energy of electrons is 0.5 MeV, and the maximum current density is 5 kA/cm^2.

Figure 7 presents the stress profiles in an iron target 1 mm thick at various times under irradiation by a pulsed proton beam with a maximum energy of particles in the pulse of 0.5 MeV and a maximum current density of 0.25 kA/cm^2. The duration and shape of the current and voltage pulses are the same as those under electron irradiation.

The solid-body part of the target occupies the region $z > 0$. The region $z < 0$ is occupied by the plasma scattered under the action of the beam. For the given parameters of the beam, the plasma temperature is 3000–6000 K. The mass density varies from several thousandths of the solid-body density at the jet front to the solid body density at the end part of the energy-release zone.

Although the electron-current density is greater than the ion-current density by a factor of 20, the maximum stress under electron irradiation is larger than the stress under ion irradiation only by a factor of 5. The fact that the stress waves generated under ion irradiation are more intense than those under electron generation is explained by the larger energy losses of ions in the material in comparison with the energy losses of electrons [26].

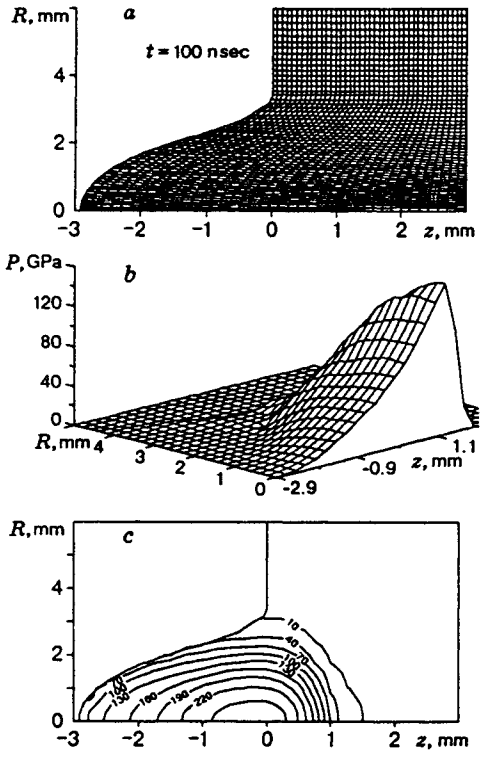

Fig. 8

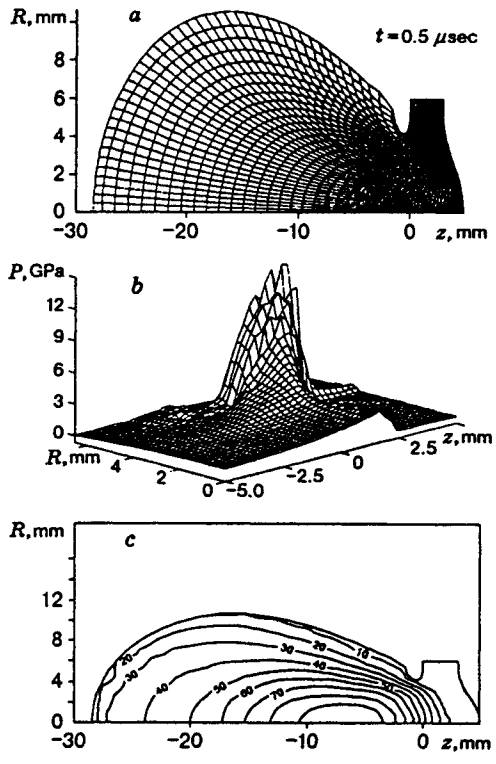

Fig. 9

It should be noted that we have failed to obtain the results presented in Figs. 6 and 7 by conventional methods (for example, by the method of macroparticles or by the Wilkins method). This is because in the examples presented, which are typical of technological applications, the irradiated part of the material is in the region of the liquid–vapor phase diagram and has a sound velocity which is 1–2 orders of magnitude less than the initial sound velocity. This leads to instability of the solution because of the "switching off" of artificial viscosity.

We present the results of the two-dimensional calculation of the action of a high-power relativistic electron beam on a thick aluminum target. The initial thickness of the target is 3 mm, the radius is 6 mm, and the initial temperature is 300 K. The electron energy is 0.5 MeV (the path of electrons with this energy in solid-state aluminum is 0.83 mm), the beam current is 180 kA, the duration of the irradiation pulse is 100 nsec, and the duration of the leading and trailing edges is 10 nsec. The radial distribution of the beam current is described by the expression $j_b(r) \sim \exp[-(r/r_b)^2]$. Here $r_b = 1.5$ mm, which ensures a maximum current density of $\sim$2.5 MA/cm^2 and a maximum power density of $\sim 10^{12}$ W/cm^2. The irradiation region was bounded by a 3-mm radius. Thus, the parameters of this beam corresponded approximately to those in the experiment of [1]. To specify the parameters more accurately, it is necessary to know the time variation of the dimensions of the focal point, which are not given in [1].

With the given parameters of the beam, the pressure jump in the energy-release zone is so great that the generated shock wave that propagates over the volume of the target gives rise to its heating and melting.

Figure 8 shows the computational grid (a), the pressure field in the target (b), and the temperature field (in kilokelvins) (c) at the end of the irradiation time. By this time, the volume of the irradiated part of the material increased by approximately a factor of 3, the maximum pressure in the target was 160 GPa, and the maximum temperature of the material reached 270,000 K. The pressure obtained here is close to that given in [1].

Figure 9 shows the same distributions as those in Fig. 8 for time 0.5 μsec. It is seen from Fig. 9a that

the region of failure of the target is much larger than the energy-release zone, which is determined by the path of particles in the target material and by the beam radius. When the shock wave reaches the free surface, this leads to melting and outflow of the material from the near-axis region and eventually to formation of a through hole in the target. The maximum of pressure is located in the peripheral solid-state part of the target (Fig. 9b), and the pressure field looks like a wave running in the radial direction. The medium's maximum temperature is approximately 10^5 K, as is seen from Fig. 9c. In the vicinity of the axis near the back part of the target, the temperature of the material is approximately 2000 K. The mass density at the front of the plasma jet amounts to less than 0.00001 of the initial density of the material, i.e., the density of the material varies by more than five orders of magnitude in the solution presented.

It should be noted that in this example, the target volume increased more than twentyfold compared with the volume, and the procedure of grid reconstruction is performed multiply by the grid generation method described in [27].

The examples presented have demonstrated high effectiveness of the method developed here for solving the equations of continuum mechanics, which allows one to simulate the dynamics of material over a very wide range of its thermodynamic parameters. This is very important in solving the problems associated with the action of high-energy beams.

The author would like to thank V. M. Fomin for his useful remarks and V. V. Val'chuk for his assistance in carrying out the calculations.

REFERENCES

1. B. A. Demidov, M. V. Ivkin, V. A. Petrov, and V. S. Uglov, "Generation of shock waves in thick targets by a high-current relativistic electron beam," *Zh. Tekh. Fiz.*, **50**, No. 10, 2205–2209 (1980).
2. V. S. Uglov, P. P. Abramov, K. G. Gureyev, and N. V. Filippov, "The effect of pulsed pressure induced by a high-power electron beam on the structure and properties of some materials," *Fiz. Khim. Obrab. Matér.*, No. 6, 144–147 (1977).
3. B. A. Demidov, M. V. Ivkin, V. V. Obukhov, and Yu. F. Timoshchuk, "Dynamic characteristics of the interaction of high-power relativistic electron beams with thick anodes," *Zh. Tekh. Fiz.*, **50**, No. 10, 2209–2214 (1980).
4. S. A. Chistjakov, A. D. Pogrebnjak, and G. E. Remnev, "Dynamical processes and changes in metal structure induced by high power ion beams," *Nucl. Instrum. Meth. Phys. Res.*, **42**, 342–345 (1989).
5. A. I. Mel'ker and I. L. Tokmakov, "Failure of solid bodies under irradiation by electrons," *Fiz. Khim. Obrab. Mater.*, No. 5, 62–68 (1977).
6. S. L. Leshkevich, V. A. Skvortsov, and V. E. Fortov, "The dynamics of failure of a metallic plate by a short-pulse ion beam," Preprint No. 6-24, Inst. Comp. Technol., Acad. of Sci., Moscow (1988).
7. S. V. Khalikov, L. V. Shelomentseva, and A. P. Yalovets, "Numerical modeling of the interaction of high-power beams of charged particles with solid-state targets," Moscow (1989). Deposited at VINITI 12.12.89, No. 7366-B89.
8. O. M. Belotserkovskii and Yu. M. Davydov, *The Method of Coarse Particles in Gas Dynamics* [in Russian], Nauka, Moscow (1982).
9. A. F. Akkerman, A. V. Bushman, B. A. Demidov, et al., "An investigation of the dynamics of shock waves induced by a high-current relativistic electron beam in aluminum targets," *Zh. Éksp. Teor. Fiz.*, **89**, No. 3(9), 852–860 (1985).
10. A. F. Akkerman, B. A. Demidov, A. L. Ni, L. I. Rudakov, and V. E. Fortov, "Application of high-current relativistic beams in the dynamic physics of high temperatures and pressures," Preprint, Department of Inst. Chem. Phys., Acad. of Sci. of the USSR, Chernogolovka (1986).
11. S. K. Godunov, A. V. Zabrodin, M. Ya. Ivanov, et al., *Numerical Solution of Multidimensional Problems of Gas Dynamics* [in Russian], Nauka, Moscow (1976).
12. V. V. Val'chuk, S. V. Khalikov, and A. P. Yalovets, "Modeling of the action of high-power beams of charged particles on layered targets," *Mat. Model.*, **4**, No. 10, 111–123 (1992).

13. M. L. Wilkins, "Calculation of elastoplastic flows," in: B. Alder, S. Fernbach, and M. Retenberg (eds.), *Methods of Computational Physics*, Academic Press, New York (1964), Vol. 3.
14. A. M. Kolchuzhkin and V. V. Uchaikin, *Introduction to the Theory of Particle Penetration Through Matter* [in Russian], Atomizdat, Moscow (1978).
15. A. V. Bushman, A. L. Ni, and V. E. Fortov, "Wide-range equations of state for metals and hydrodynamic calculations of shock-wave processes," in: *Equations of State under Extreme Conditions* [in Russian], Inst. of Theor. and Appl. Mech., Sib. Div., Acad. of Sci. of the USSR (1983), pp. 3–11.
16. S. N. Kolgatin and A. V. Khachaturyanets, "Interpolation equations of state for metals," *Teplofiz. Vys. Temp.*, **20**, No. 3 (1982), pp. 90–94.
17. B. A. Kononov, Yu. M. Stepanov, and A. P. Yalovets, "Transport of high-velocity electrons in laminated materials," *At. Energ.*, **42**, 326–328 (1977).
18. A. P. Yalovets, "A method for calculating the transport of high-velocity electrons in a material in cylindrical geometry," Moscow (1983). Deposited at VINITI 04.05.83, No. 1726-83.
19. L. V. Spencer, "Theory of electron penetration," *Phys. Rev.*, **98**, No. 6, 1597 (1955).
20. J. F. Zeigler, *Stopping Cross Section for Energetic Ions in All Elements*, Pergamon Press, New York (1977).
21. E. Oran and J. Boris, *Numerical Simulation of Reactive Flow*, Elsevier, New York (1987).
22. V. M. Fomin, V. P. Shapeev, and N. N. Yanenko, "Modeling of continuum mechanics problems with large deformations," in: *Computer Methods in Applied Mechanics and Engineering* (Holland), No. 32, (1982), pp. 157–197.
23. A. I. Gulidov and V. M. Fomin, "A modification of the Wilkins method for solving the problems of collision of bodies," Preprint No. 49, Inst. Theor. Appl. Mech., Sib. Div., Acad. of Sci. of the USSR, Novosibirsk (1980).
24. P. L. Roe, "Some contributions to the modeling of discontinuous flows," *Lect. Appl. Math.*, **22**, 163–193 (1985).
25. H. L. Brode, "The blast wave in air resulting from a high temperature, high pressure sphere of air," in: Research Memorandum RM–1825–AEC, Rand Corporation, Santa Monica, CA (1956).
26. S. V. Starodubtsev and A. M. Romanov, *Penetration of Charged Particles Through Matter* [in Russian], Izd. Akad. Nauk Uzb. SSR, Tashkent (1962).
27. Yu. P. Meshcheryakov, "A geometrical method of constructing difference grids," Preprint No. 12, Inst. Theor. Appl. Mech., Sib. Div., Acad. of Sci. of the USSR, Novosibirsk (1978).